JOURNAL OF MATERIALS SCIENCE **39** (2004) 4821–4828

Residual toughness of poly(acrylonitrile-butadiene-styrene) (ABS) after fatigue loading—effect of uniaxial fatigue loading

H. J. KWON, P.-Y. B. JAR, Z. XIA
Department of Mechanical Engineering, University of Alberta, Edmonton, AB, Canada, T6G 2G8
E-mail: hkwon@ualberta.ca

Toughness variation of non-notched poly(acrylonitrile-butadiene-styrene) (ABS) subjected to uniaxial fatigue loading was investigated. The experiments were conducted by applying fatigue loading to strip specimens first, from which dog-bone specimens were machined. The dog-bone specimens were tested to measure the strain for the on-set of fracture, named cracking strain here, thus to monitor the toughness change due to the fatigue loading.

The test results showed that the fatigue loading caused the toughness drop in ABS, even before any visible crack was developed. Damage development and fracture behavior were then analyzed using scanning electron microscopy (SEM). The SEM analysis revealed that damage zones, not cracks, were initiated during the fatigue loading, and were the main cause of the toughness drop. Mechanisms for the damage initiation include matrix crazing and debonding of small rubber particles; however, large rubber particles remained intact. Based on the results, a deformation model is proposed for the damage zone initiation, which provides an explanation for the toughness change under the fatigue loading.

1. Introduction

The increasing demand of poly(acrylonitrile-butadiene-styrene) (ABS) for load-bearing applications has required a thorough understanding of its fatigue resistance. Although most of the literature focused on the resistance to crack growth, it is the resistance to crack initiation that is important for the load-bearing applications. Early study on the fatigue resistance for crack initiation by Sauer and Chen [1, 2], using plain smooth specimens of hour-glass shape, showed that ABS deforms primarily by shear yielding, with crazes developing only at a later stage; while high-impact polystyrene (HIPS) deforms by craze nucleation and growth. Increase of rubber content in ABS was found to increase the resistance to crack propagation, but decrease the resistance to crack initiation. By modifying the testing method, Jar *et al.* [3] and Marissen *et al.* [4] reported that fracture strain of ABS decreased with the increase of the number of fatigue cycles. In particular, Jar *et al.* showed that at stress amplitude of around 67% of the tensile strength, ductility dropped 36% after only 400 cycles of the fatigue loading. This implies that for load-bearing applications, products made of ABS should not be designed to resist a load that generates normal stress of more than 50% of its tensile strength. Consistently, Marissen *et al.* [4] drew a similar conclusion that a drop of ductility occurred at the stress amplitude of 65% of its tensile strength, and concluded that ABS is sensitive to the fatigue loading. These studies, however, did not clearly show the level of the maximum fatigue stress that can be applied to ABS in product design.

It was noticed that the above two studies were based on injection-molded ABS that contained abundant gel-like defects as shown in Fig. 1a, though Jar *et al.* [5] reported that constituents of the defects are similar to those in the surrounding matrix. Marissen *et al.* [4] analyzed the defects with Raman microscopy and found that the ratios of acrylonitrile to styrene (A/S) and butadiene to acrylonitrile (B/A) in the defects appeared to be different from the ratios in the surrounding material. Nevertheless, these defects induce stress concentration in the surrounding matrix, and initiate damage.

A rational assumption that follows these studies is that by eliminating these defects, sensitivity of ABS to fatigue loading should be reduced. One of the objectives of the current study is to verify this assumption. As the defects were believed to form during the injection molding process because of the high processing temperature [5], the amount of defects in pure ABS (without any additive to raise glass transition temperature) of an extruded grade was expected to decrease significantly, due to a lower temperature required for the processing. In addition, the ABS used in the current study was specially prepared using a fine mechanical

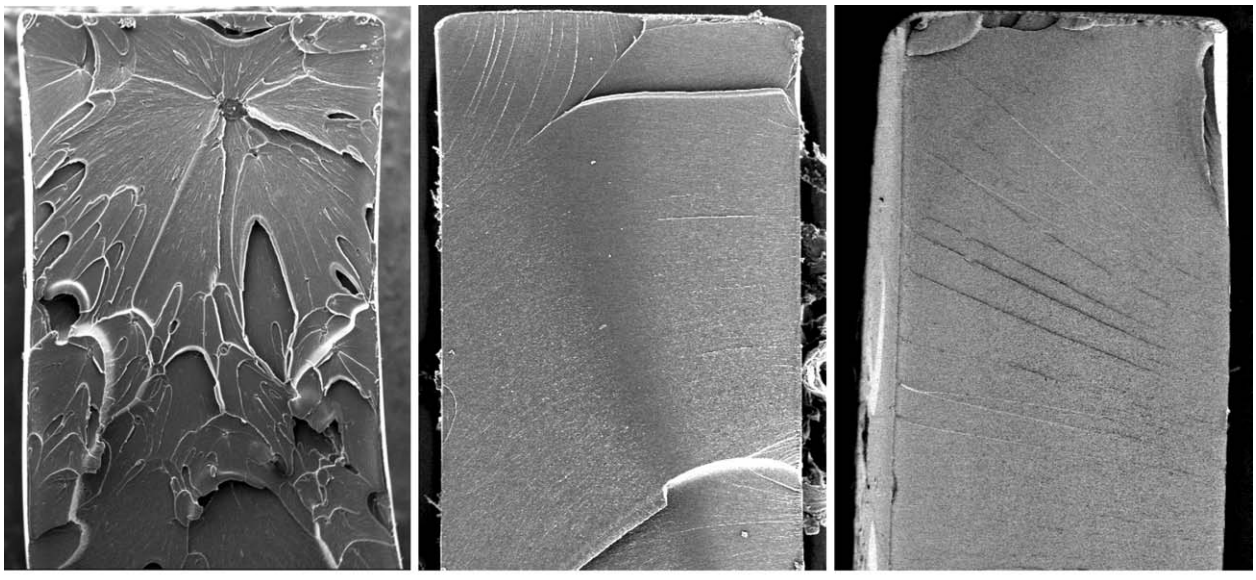

Figure 1 SEM micrographs of fracture surfaces from: (a) a tensile-fractured injection-molded specimen without fatigue loading, (b) a tensile-fractured extruded specimen after the fatigue loading at 25 MPa for 500 cycles, and (c) a tensile-fractured extruded specimen without the fatigue loading.

filter during the synthesis to remove any possibility of the defect formation. The difference is shown by the fracture surfaces in Fig. 1, in which Fig. 1a was taken from an injection molded specimen and Fig. 1b and c from specimens used in the current study. Fig. 1a clearly shows that fracture was initiated from a gel-like defect inside the specimen, and due to the interruption of crack growth by the presence of the defects, many river-flow marks are observed. However, no gel-like defects or river-flow marks were found in Fig. 1b or c that were taken from tensile fractured specimens used in the current study, with or without prior fatigue loading, respectively. Therefore, we believe that the effect of the internal defects on the fracture process has been eliminated in specimens used in the current study.

It has been noted by Marissen *et al.* [4] that presence of severe surface defects may prevent detection of the internal defects from the fracture surface. This, however, was not applicable to the ABS used in the current study, as all specimens had been carefully examined before the tensile test to ensure that there were no surface defects to dominate the fracture process.

Among the two mechanisms for fracture development under fatigue loading [6], i.e., crack initiation and propagation, the latter has been studied by many researchers using specimens containing an existing pre-crack; whereas the former has been given little attention. The conventional fracture mechanics approach also ignores the effect of the loading history on the changes of mechanical properties, except around the crack tip where the crack growth is initiated, and assumes that the properties remain constant. Results from this paper, complemented by another work from the same study [7], will be used to verify this assumption.

In this paper, effect of fatigue loading on residual fracture strain, which was measured from monotonic tensile test, is reported. Fatigue loading was firstly applied to non-notched, plain strip specimens, but the number of cycles was limited to avoid any crack or visible damage generated during the fatigue loading. Then, dog-bone specimens were machined from the strip specimens for the tensile tests, to evaluate the change in strain for the on-set of fracture (to be named cracking strain here). The cracking strain is used as an indication of the change in toughness caused by the fatigue loading.

2. Experimental

2.1. Material and specimen preparation

An extrusion grade ABS was used for the study. The extruded ABS plates had dimensions of 300×300 mm^2 in size with nominal thickness of 3.2 mm, provided by Denki Kagaku Kogyo Co. Ltd., Japan. Rubber particles in the ABS have a bi-modal particle size distribution [8, 9], one around 1 μm in diameter and the other 0.1 μm. Preliminary tensile tests showed that the extrusion process did not introduce any orientation effect that would have affected isotropy of its mechanical properties. The preliminary test results also suggested that the ABS has tensile strength of 50 MPa and Young's modulus 2.5 GPa. As shown by the tensile fracture surface in Fig. 2, from an ABS specimen of original thickness, the fracture surface contains virtually no gel-like defects.

Procedure of the experimental study is described in Fig. 3 and the specimens used for this study are shown in Fig. 4. Strip specimens of 25×145 mm^2 were machined from the plates for the uniaxial fatigue tests, after which dog-bone specimens were machined for the subsequent tensile tests, to remove potentially damaged corners along the specimen edges due to the fatigue loading. The level of fatigue loading was in the range of 30% (15 MPa) and 60% (30 MPa) of the original tensile strength. Even though the plates were extruded, the preliminary tests suggested that the anisotropy was very negligible. Therefore, the ABS was regarded as

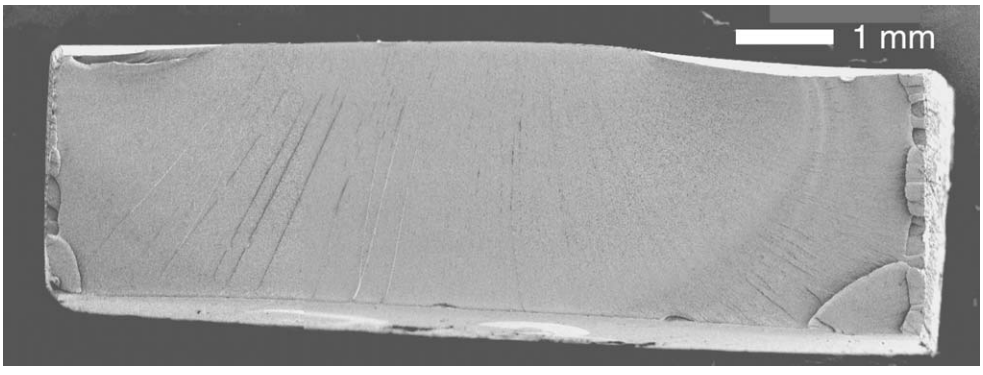

Figure 2 Tensile fracture surface of an ABS specimen, showing no evidence of the gel-like defects that were observed by Jar *et al.* [3] and Marissen *et al.* [4].

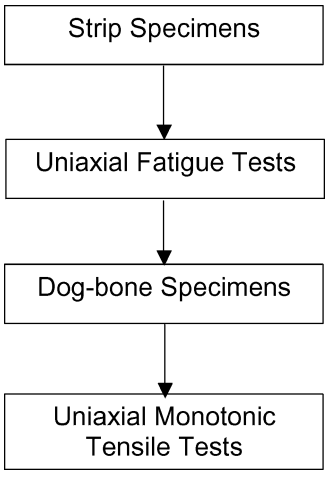

Figure 3 Schematic diagram for the experimental procedure.

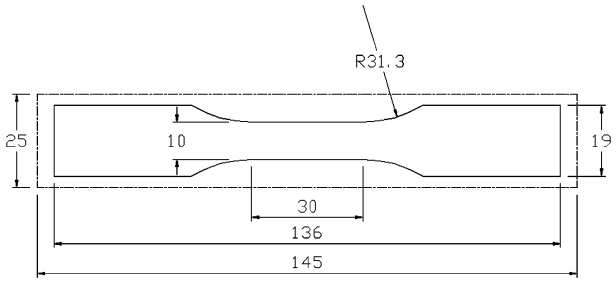

Figure 4 Over-all dimensions of the strip specimen (as outlined by the broken line) used for the fatigue loading and the relative position and the dimension of the dog-bone specimen (solid line) for tensile test. The relative position of the two types of specimens is demonstrated in the figure.

isotropic in mechanical properties. Final dimensions of these strip specimens for fatigue loading were machined using a milling process, and then polished with 400- and 600-grit wet sand papers. Surfaces across the width of the ABS strips were not machined, nor polished, and the strip specimens were handled with an extreme care to ensure that no scratches were introduced on the surfaces during the machining.

After the fatigue tests, dog-bone specimens were machined from the strip specimens for the tensile test. Width and length in the gauge section of the dog-bone specimens were 10 and 30 mm respectively and the neck region had a radius of 31.3 mm. Dimensions of the two types of specimens and their relative positions are shown in Fig. 4.

To ensure that tensile fracture would occur in the gauge section, central width of the gauge section was reduced by 0.1 mm (1% of the width), following the recommendation in ASTM standard [10]. The width reduction was achieved through hand polishing using 400- and 600-grit wet sand papers with the guide of a polishing jig to ensure consistency of the dimensional reduction.

2.2. Mechanical tests

Uniaxial fatigue tests were conducted using a hydraulic testing machine, MTS Series 812, at a frequency of 0.1 Hz, under load control with the full range of 4455 N (1,000lb$_f$). A loading function, "Haver" sine wave that is from 0 to a pre-determined force level in a sinusoidal form, was applied to generate the desired fatigue loading. In the rest of the text, the peak forces used for the fatigue tests were expressed in terms of the percentage of the original tensile strength (50 MPa), that is, 30, 40, 50, and 60% for the applied stresses of 15, 20, 25, and 30 MPa, respectively. In this range of fatigue loading, 500 cycles were found sufficient to detect the toughness change. It should be noted that at a loading level above 60% of the tensile strength (30 MPa), fracture or clearly visible cracks occurred before 500 cycles were reached, thus not suitable for this study. More than 15 specimens were used for each of the loading conditions, from which results were averaged and reported here, with standard deviation showing the scattering level among the data points.

A universal screw-driven testing machine, made by Instron, was used for the tensile test, at a ram speed of 5 mm/min (0.2 inch/min), conforming to the range of testing speed specified in the ASTM Standard [10]. The deformation was measured using an extensometer with an initial gauge length of 25.4 mm (1 inch).

It should be noted that the range of fatigue loading used in this study did not affect the maximum tensile stress or Young's modulus of the dog-bone specimens. Fig. 5a and b show the typical tensile stress-strain curves of the original and fatigued specimens. The only change caused by the fatigue loading was the strain at the on-set of fracture, named "cracking strain." The cracking strain was determined by the intersection of

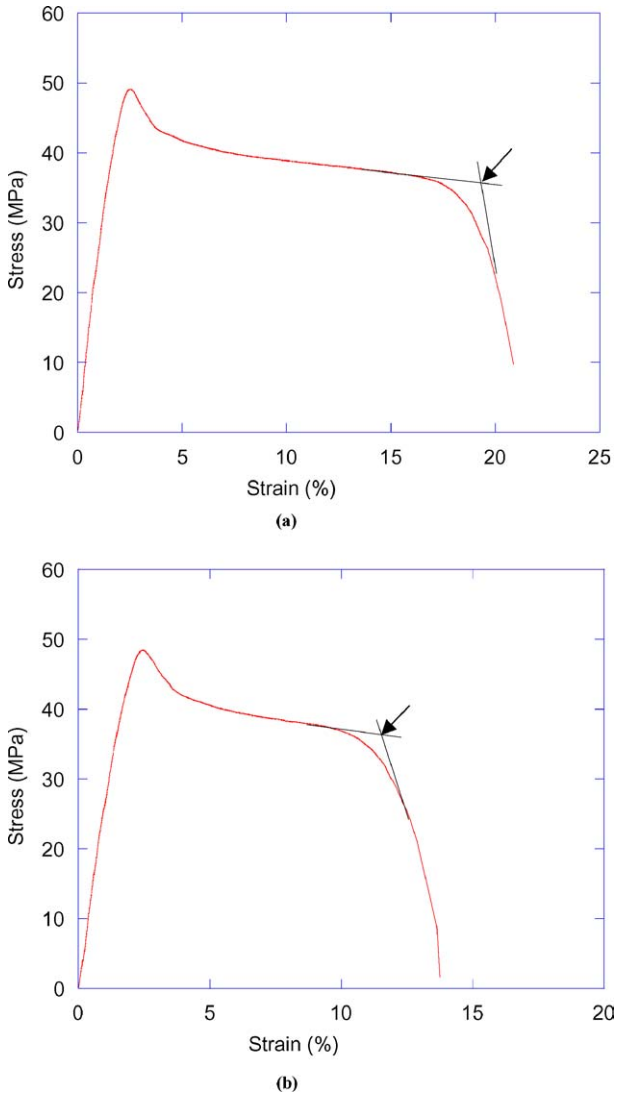

Figure 5 Typical stress-strain curves from tensile tests: (a) after the fatigue loading at 20 MPa for 500 cycles, and (b) without the fatigue loading.

two straight lines that are tangential to the plastic drawing section and the final fracture section of the curve, respectively, as pointed by arrows in Fig. 5. In the following section of Results and Discussion, the cracking strain will be used as a measure of the toughness change by the fatigue loading.

2.3. Scanning electron microscopy

A Jeol scanning electron microscope (model JSM-6301F) was used to investigate the fractured surface after the tensile test. Each of the specimens of interest was mounted on a sample holder and then coated with a thin layer of gold just before the SEM examination.

3. Results and discussion

3.1. Mechanical test

Summary of the cracking strains after various uniaxial fatigue loadings is presented in Fig. 6 in which a dashed line is used to show the trend. The very left point in the figure (♦ at 0 MPa) is the cracking strain from non-fatigued specimens. All the other points of the solid

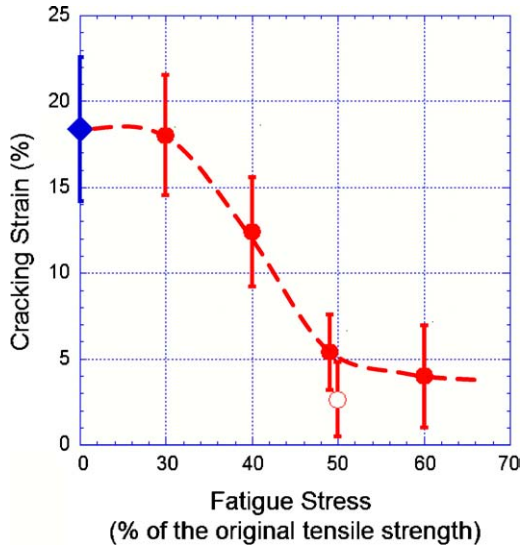

Figure 6 Summary of the variation of fracture strain and standard deviation as a function of the peak stress value under the uni-axial fatigue loading for 500 cycles. Filled circles (●) were from specimens with the original thickness of 3.2 mm, and open circle (○) from the reduced thickness of 1.28 mm.

symbols (●) are from specimens of original thickness under 500 cycles of the specified fatigue stress levels. As shown by the dashed line, a distinct drop of the cracking strain occurred when the fatigue stress was above 30% of the original tensile strength, and then leveled off to less than 25% of the original cracking strain at a fatigue stress level above 50% of the original tensile strength.

The results clearly suggest that a significant reduction in toughness was introduced by the fatigue loading at a stress level lower than 50% of the tensile strength, though no gel-like defects were detected. The results also showed a strong relationship between residual ductility and fatigue loading, which should be considered in load-bearing applications. Additional fatigue tests, up to 5,000 cycles, confirmed that 30% of the tensile strength is the threshold fatigue stress, below which the cracking strain is not changed by the fatigue loading. Therefore, design stress for ABS in load-bearing applications should not exceed 30% of its tensile strength.

It should be noted that at a fatigue stress level above 60% of its original tensile strength, stress whitening appeared around the specimen edge during the 500-cycle fatigue loading, and at a fatigue stress level equivalent to 70% of the tensile strength the specimens fractured before 500 cycles were reached. Therefore, 60% of the tensile strength should be very close to the maximum fatigue stress allowed for 500 cycles. This critical stress level is lower than that expected for the injection-moulded ABS, as no visible whitening or cracks were found in the latter even after 1000 cycles of fatigue loading at 67% of its tensile strength [3]. Marrissen *et al.* [4] also anticipated a much longer fatigue lifetime at a loading level higher than that reported here.

Apart from material parameters such as molecular weight and rubber content that may have affected the maximum allowable fatigue stress level for 500 cycles, one possible factor that is related to product design for

load bearing applications is the specimen surface condition. In principle, surface finish by injection molding should be no different from that by extrusion. However, extruded plates are relatively large in size, compared to the injection-molded dog-bone specimens, and through stacking and handling for transportation, the former are more likely to have surface scratches. In addition, the relatively open environment for the extrusion process means that extruded plates are prone to having contaminants deposited on the surface, which act as stress concentrators during loading. The extruded plates used in this study had also experienced additional handling processes, such as for machining to make strip and then dog-bone specimens. The dog-bone specimens used in the previous studies, on the other hand, were formed directly from the injection-molding process. Therefore, it is very likely that the surface conditions for specimens used in this study was not as good as that for the previous studies, which may have lowered the maximum allowable fatigue stress level.

The above possibility was investigated by milling down the specimen thickness from 3.2 to 1.28 mm, and then tested at the fatigue stress level of 50% of the tensile strength. To improve consistency of the results, the milled surface was polished using wet sand papers of 400- and 600-grit. Compared to the extruded surfaces, the resulted surface finish of the specimens with reduced thickness was slightly worse. The open circle ($\circ$) in Fig. 6, with the standard deviation, presents average of the test results from specimens of the reduced thickness. As shown in the figure, the increase in surface roughness has reduced the cracking strain values, in support of the above discussion.

The relatively close positions between the open circle and the solid circle in Fig. 6 at the same fatigue stress level also suggest that the drop of cracking strain, depicted by the dashed line, was not due to the difference in surface roughness of specimens used in these test conditions.

3.2. SEM examination

The overall observation from the SEM examination is that the fracture surfaces consisted of four phases of the fracture development, similar to that suggested by Meguid [11]. Fig. 7a is the SEM micrograph from a specimen that fractured at a cracking strain of 3.5% in the tensile test after 500 cycles of uniaxial fatigue loadings at 50% of the tensile strength, i.e., 25 MPa. This is the typical fracture surface of specimens after fatigue loading above 40% of the tensile strength (20 MPa) that caused a significant drop of the cracking strain. The fracture surface in Fig. 7a contains a diagonally shaded band, with ends of the band marked by D and D′, from the top middle edge towards the bottom left corner. The band represents the border between regions developed by slow and fast crack growth, respectively, during the tensile test. Fig. 7b is a SEM micrograph from the circled region A in Fig. 7a, which shows a typical tearing pattern that represents shear-deformation-dominated fracture during the tensile test [12]. Rubber particle cavitation is clearly visible in Fig. 7b, consistent with that reported by Jar *et al.* [3]. On the other hand, in the fast crack growth region, as circled and marked by B in Fig. 7a, the fracture pattern has a relatively flat feature with most of the rubber particles fractured in a cleavage manner, as shown in Fig. 7c. Based on the observation, the dominant fracture mechanism in region B is believed to be crazing. Therefore, the band D-D′ in Fig. 7a must have been generated by the transition of the deformation mechanisms, from shear deformation in region A to crazing in region B. Crack growth through shear deformation is believed to be a relatively slow process, comparing to the crack growth through crazing that has led to ultimate fracture of the specimen.

Fig. 7d and e present two SEM micrographs from the region circled and marked by C in Fig. 7a. This region could only be found in specimens after fatigue loading, thus must have been generated during the fatigue loading. At a low magnification, Fig. 7d, the fracture surface shows stream-lines that are in a direction perpendicular to the edge of the fracture surface. Since the direction of the stream-lines represents the crack growth direction, fracture in this region is believed to have started from the edge of the fracture surface, that is, the fracture was initiated from the original surface of the ABS plates. A small shaded band can be found in the central right part of Fig. 7d, inside which the fracture surface is magnified in Fig. 7e. The fracture behavior in Fig. 7e is apparently different from that shown in Fig. 7b and c in that a significant number of small rubber particles, of 0.1 μm in diameter, were found on the fracture surface and the majority of the large rubber particles, of around 1 μm in diameter, were fractured in a cleavage manner. We believe that the small rubber particles were debonded from the matrix during the fatigue loading, which is consistent with that suggested in a previous study [3].

Although the region C in Fig. 7a was initiated during the fatigue loading, we believe that the fatigue loading did not create a crack, as striations that would have been generated by fatigue crack growth could not be found in any of the fatigued specimens. Possibility of a crack being generated by the fatigue loading was also excluded based on the fact that size of all damage zones was limited to 25 μm, which was too small to include any crack growth. Deformation in region C during the fatigue loading is believed to have involved only debonding of the small rubber particles and crazing of the matrix.

By comparing the fracture behaviors in different regions, as presented by the micrographs in Fig. 7, we conclude that the following deformation mechanisms were involved in different stages of the fracture process. In the initial damage development stage by the fatigue loading, debonding of small rubber particles and matrix crazing, as shown in Fig. 7e, occurred from defects nearby the specimen surface. In the following tensile test, cracks were then generated from this damage zone by cleaving the large rubber particles and breaking down the craze fibrils. Further crack growth in the tensile test was dominated firstly by shear deformation and rubber particle cavitation, as shown by Fig. 7b, and then

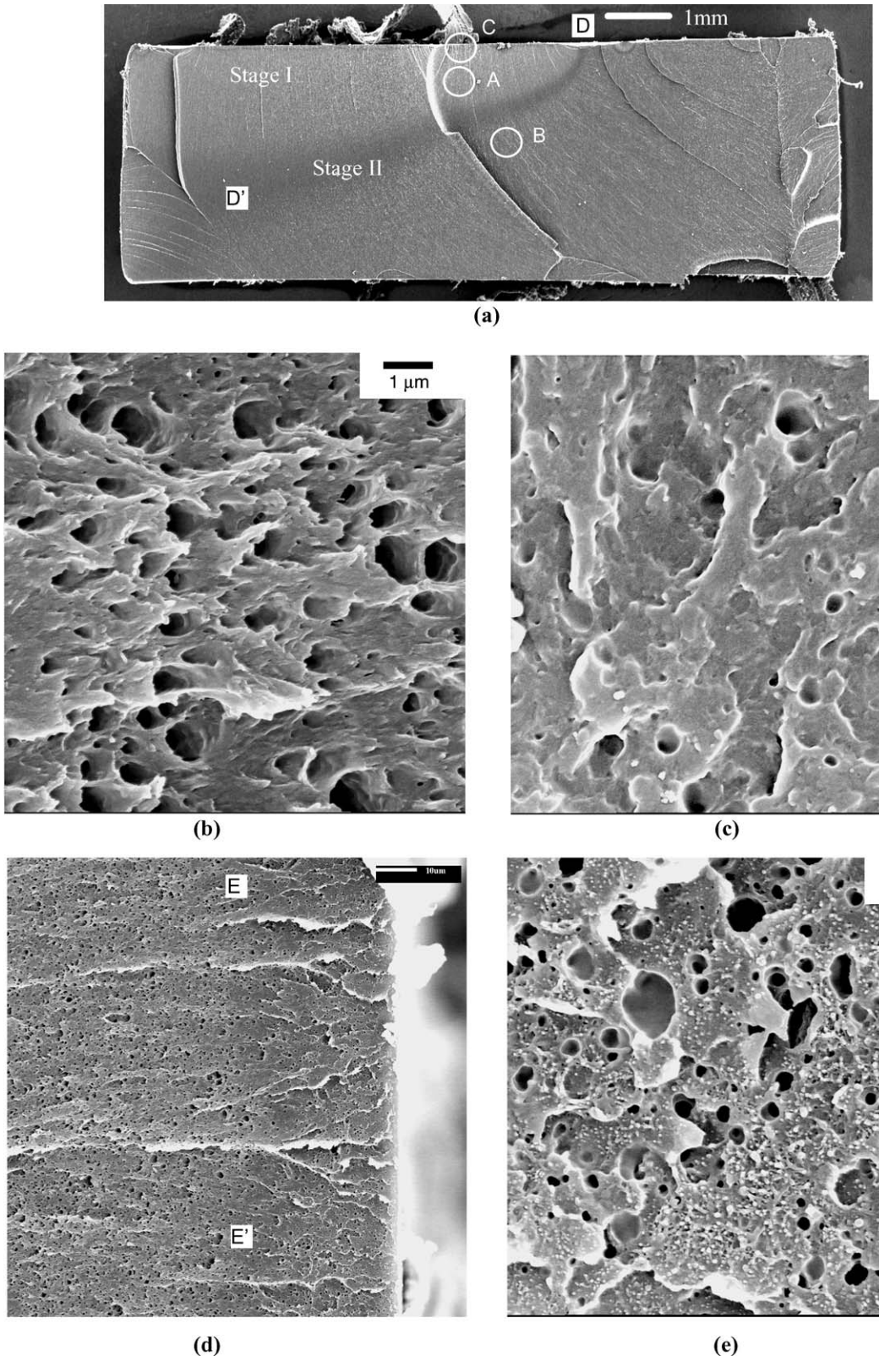

Figure 7 SEM micrographs: (a) at low magnification to show the over-all tensile fracture surface after uni-axial fatigue loading at 25 MPa for 500 cycles (A, B and C mark regions for the following micrographs), (b) from region A, (c) from region B, (d) low magnification from region C (after being rotated 90° clockwise), and (e) high magnification from region C.

by fast fracture due to crazing and particle cleavage, as shown in Fig. 7c.

A model presented in Fig. 8 depicts the deformation initiated by the fatigue loading. The model suggests that due to large local strains generated by crazing, which has been estimated to be more than 100% [13] with craze width around 0.1 μm [14], the small rubber particles were unable to adhere to the matrix, thus debonding occurred. However, for large rubber particles of 1 μm in diameter, a much smaller over-all strain was needed to accommodate the deformation caused by the craze formation. Thus, the large particles remained intact during the fatigue loading. Since the craze fibrils are aligned packets of

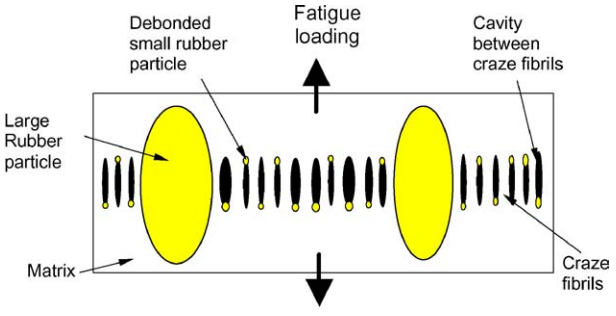

Figure 8 A deformation model for the damage zone development.

molecular chains that can carry much higher stresses than the molecules in an un-deformed state, the tensile strength of the fatigued specimens did not show any drop. The shaded band E-E′ in Fig. 7d is believed to represent the end of the fatigue-damaged zone (to be abbreviated as "damage zone" in the rest of the text).

The fracture surface represented by Fig. 7d and e was eventually formed during the tensile test by breaking down the craze fibrils and cleaving the large rubber particles, in a manner similar to those occurred in the craze-dominated region in Fig. 7c.

Initiation of a damage zone is believed to be from defects that could be either scratches or contaminants on the specimen surface. For injection-molded specimens, initiation of the damage zones was dominated by the internal defects [3, 4]. Thus, the damage zones were found all over the cross section. For the extruded ABS used in this study, the internal defects were virtually non-existent. Therefore, damage zones were all initiated from the specimen surfaces. As such, the continuous drop of the cracking strain that had been observed in the injection-molded ABS [3, 4] did not occur in the extruded ABS. Instead, a step-wise change of toughness was observed, as shown by the change of cracking strain in Fig. 6.

To further study the effect of the damage zone on the cracking strain, SEM was used to investigate the fracture surface of another specimen (named F-2, Fig. 9) that showed a very different cracking strain from that for Fig. 7a (named F-1). Specimens F-1 and F-2 underwent the same fatigue loading (25 MPa for 500 cycles), but the resulting cracking strain for the former was 3.5% and the latter 10.5%. As shown by the two fracture surfaces, Fig. 7a for F-1 and Fig. 9 for F-2, difference of the cracking strains is reflected by the fracture surface topography. Fig. 7a contains several damage zones, but Fig. 9 contains only one damage zone. This strongly suggests that the cracking strain value is closely related to the number of the damage zones generated during the fatigue loading, i.e., fatigue loading that generates multiple damage zones also causes further reduction in the cracking strain. This suggests that control of the surface defects, either surface scratches or contaminants, is an important factor to avoid fatigue-induced toughness reduction in the ABS.

4. Conclusions

The toughness change of ABS under fatigue loading was investigated using non-notched specimens, machined from extruded plates. It was found that the toughness drop can occur in ABS under fatigue loading even before any crack was developed. This toughness drop came from small damage zones that were initiated during the fatigue loading at a stress level higher than 30% of the tensile strength. Most of the damage zones were initiated from specimen surfaces, which is different from that observed in the injection-molded specimens where internal defects were the main source for the damage initiation.

A deformation model was presented for the damage zone generation. The model suggests that the damage zone was initiated from surface defects, and contained matrix crazes and debonded small rubber particles of 0.1 μm in diameter. Large rubber particles of 1 μm in diameter did not fracture during the fatigue loading, but were cleaved in the following tensile tests, along with the formation of matrix cracks that eventually led to the final fracture.

The study suggests that the maximum level of applied stress for ABS should not exceed 30% of its tensile strength. Above this stress level, ductility of the ABS can drop dramatically even after a very small number of cyclic loading.

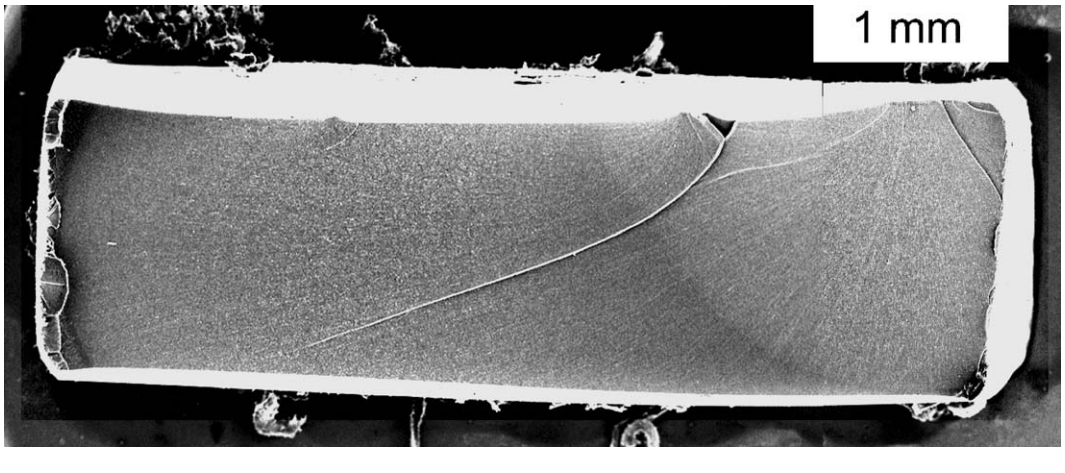

Figure 9 SEM micrograph of the over-all tensile fracture surface of specimen F-2 after uni-axial fatigue loading at 25 MPa for 500 cycles.

Acknowledgement

This work was sponsored by Natural Sciences and Engineering Research Council of Canada (NSERC). We are grateful to B. Faulkner and A. Yuen in the Department of Mechanical Engineering, University of Alberta for the technical assistance in mechanical testing and Dr. Lee in Dept. of Earth and Atmospheric Science for the SEM examination.

References

1. J. A. SAUER and C. C. CHEN, *Adv. Polym. Sci.* **91/92** (1990) 69.
2. *Idem.*, *ibid.* **52/53** (1983) 169.
3. P.-Y. B. JAR, K. KONISHI and T. SHINMURA, *J. Mater. Sci.* **37** (2002) 4521.
4. R. MARISSEN, A. V. J. KEMP, S. M. H. COOLEN, W. G. DUIZINGS, A. VAN DER POL and A. J. VAN GULICK, *ibid.* **36** (2001) 4167.
5. P.-Y. B. JAR, A. J. BERRY, K. KONISHI and T. SHINMURA, *J. Mater. Sci. Lett.* **20** (2001) 655.
6. J. P. TROTIGNON, *Int'l. Polym. Sci. Tech.* **20**(2) (1993) T67.
7. H. J. KWON, P.-Y. B. JAR and Z. XIA, in Proceedings of 19th Canadian Congress of Applied Mechanics, Calgary, June 2003, edited by M. Epstein *et al.* (2003) 128.
8. E. H. ROWE and C. K. RIEW, *Soc. Plastic Eng. Annual Tech. Conf. Paper* **20** (1974) 663.
9. *Idem.*, *Plastics Eng.* **31** (1975) 45.
10. Standard Test Method for Tensile Properties of Plastics, D 638-01, Annual Book of ASTM Standards.
11. S. A. MEGUID, "Engineering Fracture Mechanics" (Elsevier Applied Science, London, 1989) p. 76.
12. C. B. BUCKNALL, "Toughened Plastics" (Applied Science, London, 1977) p. 137.
13. A. M. DONALD and E. J. KRAMER, *J. Mater. Sci.* **17** (1982) 2351.
14. R. P. KAMBOUR and R. W. KOPP, *J. Polym. Sci.* **A-2 7** (1969) 183.

Received 5 October 2003
and accepted 31 March 2004